MECHANICAL TESTING AND SHIPPING DEVELOPMENT CONCERNING DIRC BaBar DETECTOR COMPONENTS

June 2015 - Indiana University Department of Physics

Efforts to study the successful integration of four DIRC BaBar detector modules into the GlueX Experiment have been a primary focus for the team at Indiana University during 2014-15. Several challenges to that incorporation have been examined in a detailed manner. Those challenges include vertical versus horizontal orientation of the detectors, a suitable support framework concept, and a reliable shipping container system, to prevent any damage to the bar boxes during transport.

END WINDOW AND WEDGE LOAD TEST

One of the primary mechanical concerns regarding the vertical orientation of the DIRC bar boxes involves the strength of the box end window and bar wedges shown in Figure 1. The components in question are made of Corning 7980 fused silica, with a Modulus of Rupture of 7600 psi, abraded. The window physically measures 4.882 inches * 17.205 inches * .377 inches thick. The unsupported dimensions of the window are 16.732 inches * 4.508 inches (the working window area).

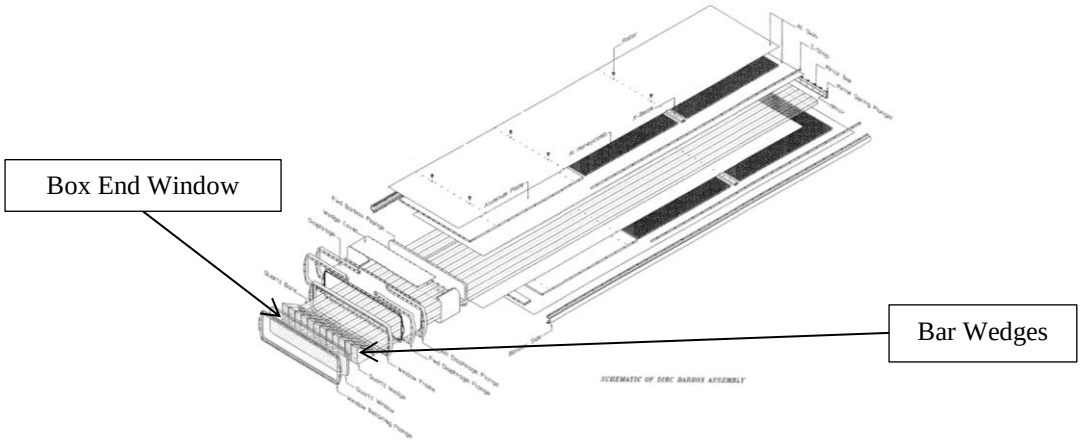

Figure 1 – DIRC Bar Box Assembly, showing end window and bar wedges

There are two primary forces that would act upon these parts in the vertical orientation, the weight of the fused silica bars and the spring pressure applied to the mirrors on the opposite end of the box. Both act downward towards the window, along the long axis of the box. Of the twelve silica bars contained in each bar box, each bar section weighs approximately 14.5 lbs. The maximum spring force applied in the bar boxes is 1500 N or 338 lbs. total. Divided evenly among twelve bars makes for approximately 28 lbs. per bar. Thus the total force on each bar is around 43 lbs. The force is transmitted from the bars to the window through the wedges epoxied to the ends of the bars and the face of the window, as shown in Figures 1 & 2.

Due to numerous variables it is a little unclear how the geometry of the wedge will affect the distribution of the pressure from the bars to the window. While it is certain that the pressure will not be evenly spread across the entire face of the wedge, at the same time it is doubtful that

the force will remain completely concentrated under the bars. Figure 2 is a section view of the working bar boxes and shows the geometrical relationships between the window, wedges, and bars. Also labeled are parts referred to in the next section.

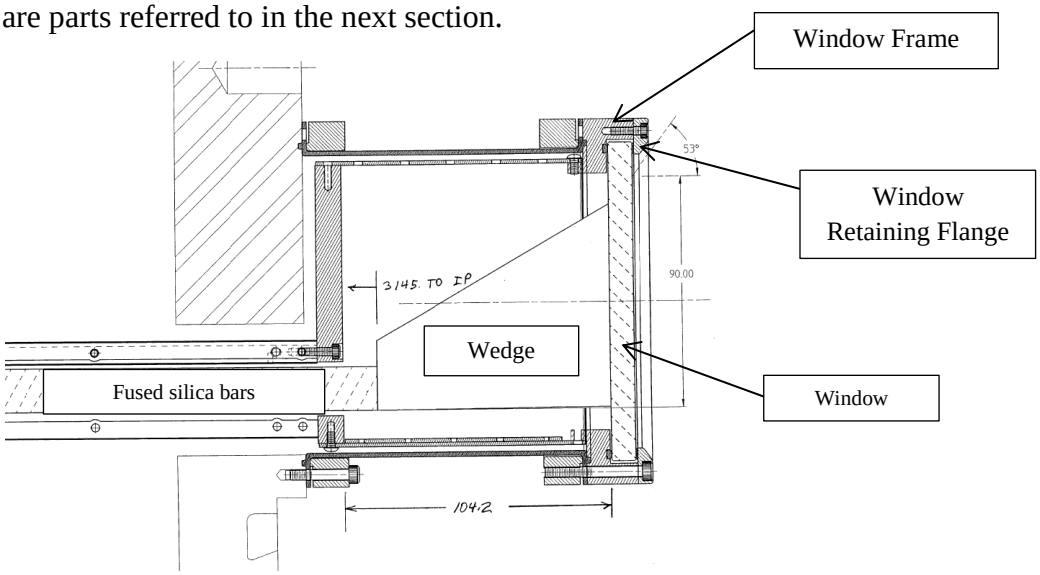

Figure 2 – Section view of bar box at window end

In order to closely replicate the nature of the existing bar boxes, a test setup as shown in Figure 3 is proposed. Copies of the stainless steel window retaining flange and window frame used on the bar boxes will be machined, to hold the silica window in place. The interface between these parts and the window consists of an O-ring and an EPDM rubber gasket, which are included. Mock wedges will be machined from aluminum to replicate the geometry of the silica versions. In the center of the window where the stress is expected to be the highest one or two fused silica wedges will be installed. The mission of these silica wedges is to observe any damage that might occur to the edges of the wedge, where FEA models have shown elevated stress concentrations. The base of the set-up is a sturdy W6 steel beam, which will prevent unintended deflection outside of the test area.

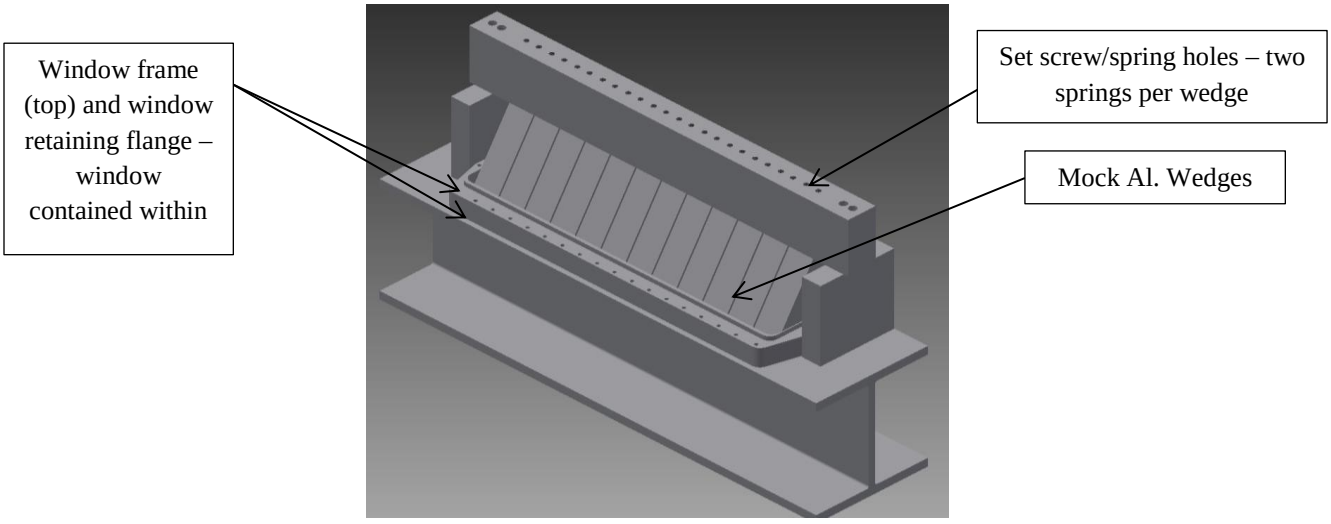

Figure 3: Fused Silica Window Load Test Set-Up

To evenly apply the required load each wedge will be put in compression by two die springs trapped above in bores drilled in a rectangular steel beam. These springs will be compressed using 5/16-18 set screws and ball bearings. Since the die springs have known spring rates, their load rating at a specific compressed length is given by the manufacturer. Springs with a load rating of 42 lbs. (compressed) have been chosen for the test. Employing two of these springs on each wedge will allow an approximate 2X force to be applied.

Several finite element analyses have been performed on the CAD models for this project, and all have given fairly large safety factors regarding the window and surrounding parts. FEA models include the window, retaining flange, window frame and wedges. The highest observable stress in the models has been approximately 1525 psi, much below any yield strength for the materials involved. This figure is for the working load of 42-43 lbs. per bar/wedge element. The measured stress in the window typically is one of the lowest stressed areas of the whole model. Typically the high stress points were on the leading edge of the wedge components, near the interface with the window.

One point of variance that was introduced into the simulation was the interface between the wedges and the silica window. In the functioning bar boxes this interface is a solid joint bonded with Epo-Tek 301-2 optical epoxy. In the proposed strength test described above the interface is simply a sliding contact surface; that is, the wedges are not bonded to the window. We were interested in how this variance would impact the tests results and thus performed both simulations. Below in Table 1 are the results of those simulations. The results under "bonded" describe the simulation where the wedges were constrained to the window. "Sliding-no separation" describe the dry, non-bonded joint.

Table 1 – FEA Test Values for Wedge-Window Simulation

LOAD-JOINT TYPE (LBS.)	HIGHEST OBSERVED STRESS IN MODEL (PSI)	MAXIMUM MODEL DISPLACEMENT (INCHES)	MINIMUM SAFETY FACTOR
43 lbs. (1X) – sliding no separation	1,526	8.3 EE -5	15+
86 lbs. (2X) – sliding no separation	3,053	1.7 EE -4	10.39
43 lbs. (1X) – bonded	1,206	6.7 EE -5	15+
86 lbs. (2X) – bonded	2,412	1.3 EE -4	11.39

From the simulation results it appears that the 200% load "sliding – no separation" test is a worse-case scenario, as the highest observed stress is 23% higher than the "bonded" test of the same loading. The above values are for all aluminum wedges. When silica wedges are introduced, the safety factor generally drops a couple of factors. Repeated simulations show stress points on the tip of the wedges near the interface with the window. The concentrations occur there as the components react to the simulated load and the pressure tends to shift towards specific contact points on the wedge face.

One manual calculation that is readily available by glass manufacturers is a formula that produces the required thickness for pressure windows. The equation is as follows:

$$\text{Window thickness} = t = l * w * \sqrt{\frac{P*K*SF}{2*M*(l^2+w^2)}}$$

Where:

l = length of unsupported window = 16.732 inches
w = width of unsupported window = 4.508 inches
P = uniform pressure on window
K = empirical constant for edge condition = .75 for clamped edge
SF = safety factor, commonly 7 or better
M = modulus of rupture = 7600 psi

Obviously the pressure is not uniform in this particular case due to the wedge geometry, yet it is helpful to run through the calculation for reference. If the force from the bars was transmitted uniformly across the whole surface of the wedges to the glass, the pressure would be around 10.3 psi. Rearranging the equation to solve for safety factor, rather than thickness, we get:

$$SF = \frac{2*M*(l^2+w^2)*(\frac{t}{l*w})^2}{P*K}$$

Using .377 inches for the window, we arrive at a safety factor of 14.8.

It is felt that a 200% test load on the window will provide some physical assurance that the detector modules can be vertically oriented safely. While the available simulations seem to point to a healthy factor of safety, applying a 2X load in practice will help reinforce that position. As was mentioned in the calculation above, a common safety factor of 7 is used in many pressure window applications. It would appear this situation has provided a much higher factor than 7, yet a practical test would be reassuring. If handled carefully during installation and use, the window and wedges should not experience a 200% loading outside of an uncontrolled event. Concerning the wedges the stresses observed in the FEA models have been relatively low with the exception of the leading edges, where maximum stress has been within 4-5 factors of safety in the 200% models. Localized material failure in these areas would most likely not cause the entire wedge to fail. However we have chosen to include one or two silica wedges in the test to see if any micro fracturing takes place under the 200% test. There is also a good chance that the elevated stress points witnessed in the FEA models could simply be modeling error, another reason to include silica wedge samples.

TEST RESULTS

Figure 4 – Window Pressure Test Set-Up at full load

During the final week of 2014 the window pressure test set-up was assembled, and was then allowed to sit fully loaded for over two weeks during the holiday break. All components were thoroughly cleaned prior to assembly, to ensure all grit and dirt was removed.

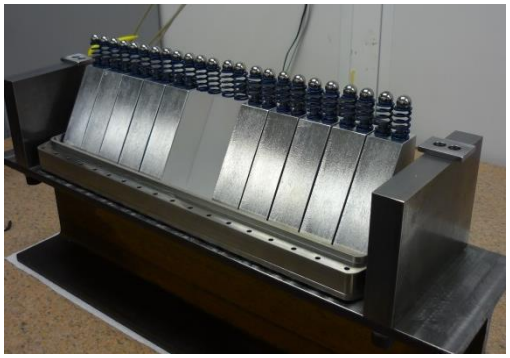

Figure 5 – Test Set-Up, springs in place over wedges during initial assembly

Once the wedges were set on the window surface, the die springs were set in place along with the ball bearings. The steel beam was then set down over the springs and fastened in place. The set screws were adjusted until they just made contact with the bearings. At this point a measurement was taken, using a height gage and dial indicator, of the initial location of the top of each screw. Once the screws were fully tightened they were re-measured to ensure a sufficient amount of compression on each spring had been attained. Each screw was tightened in half turn increments uniformly across the beam, to attempt to load the window as evenly as possible.

After two weeks the window was unloaded, by backing the set screws off in the same manner they were tightened. There was no visible damage to any of the wedges, window, or flange components. The gasket and O-ring both were free of any damage.

Figure 6 – Window, flanges and gasket following pressure test

HORIZONTAL FRAME CONCEPT

From the standpoint of safety concerning the end windows in the bar boxes, a horizontal orientation during use in the GlueX Experiment appears most prudent. The boxes were originally designed for horizontal orientation while in use with the BaBar Experiment. The BaBar detector held the bar boxes in a series of tracks, in which corresponding bearings on the bar boxes roll and guide the boxes during assembly.

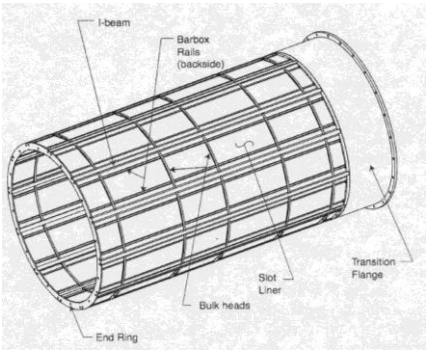

Figure 7 Schematic of BaBar Central Support Tube, showing bar box rails

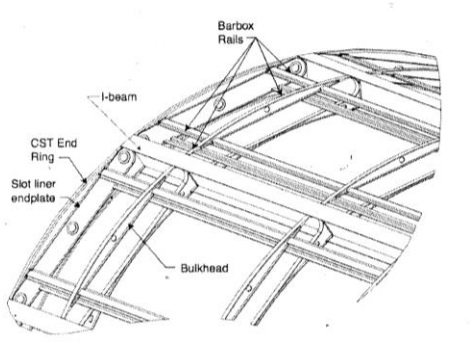

Figure 8 Detail schematic of the BaBar Central Support Tube, showing the relationship between the bar box rails and surrounding components

The original BaBar detector held the bar boxes in a radial arrangement, around a Central Support Tube. The rails supporting the bar boxes were affixed in the detector by lightweight aluminum bulkheads, themselves supported by aluminum I-beams. Thin aluminum sheet covered both

sides of the support tube, further adding strength. The proposed concept design for the GlueX support structure shares many of these features. Much of the Central Support Tube was assembled using a durable two part epoxy, in lieu of mechanical fasteners. This included the joint between the bar box rails and the aluminum bulkheads. To insure proper alignment of the bar box rail sections, the rail components were held within the bulkheads by fixtures and epoxied in place. It is proposed that similar assembly procedures used for the Central Support Tube eventually be used on the GlueX horizontal support structure.

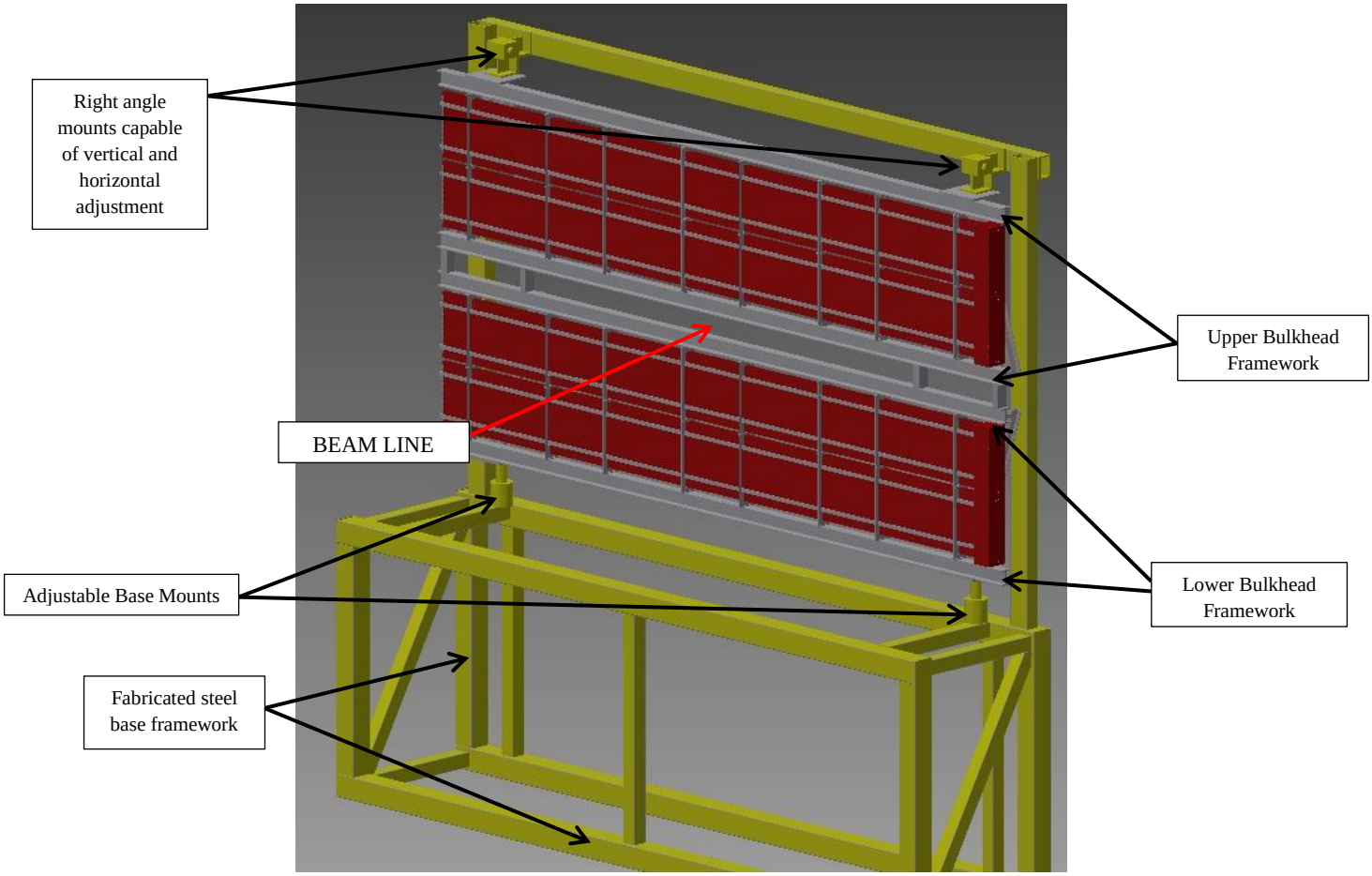

Figure 9 Proposed Concept GlueX Bar Box Support Structure (Bar box mock-ups shown in position)

The proposed GlueX support structure consists of two bulkhead frameworks, stacked one atop another. The frames are centered vertically and horizontally on the beam line. Aluminum I-beams form the outer perimeter of each bulkhead framework. Each of the frameworks is structurally independent of one another, and will be constructed separately. The connection between the frameworks is made by simple risers, which bolt to the I-beams and separate the frames to allow the beam to pass between. Once connected and the bulkhead frames become one assembly, they attach to the steel support frame by means of adjustable base mounts and right angle mounts, similar in design to those currently used on the Hall D Forward Calorimeter. In this manner the whole assembly can be adjusted as one, in situ to achieve the final placement in the beam line.

To compensate for inherent misalignment in the beams, bar box rails, etc. it is proposed that the connection between the I-beams and the bulkheads incorporate a T-slot, as shown in Figure 10. When the bar box rails are attached to the bulkheads a fixture will maintain the distance between the rails (gauge), thus sufficient accuracy and precision should be fairly attainable in that respect. However any lateral bowing in the I-beams or tracks would be more difficult to eliminate pre-assembly. T-slots would allow the bulkheads to be adjusted to eliminate binding in the rail-bar box bearing interface, whether it be from I-beam bowing, lateral track misalignment, etc.

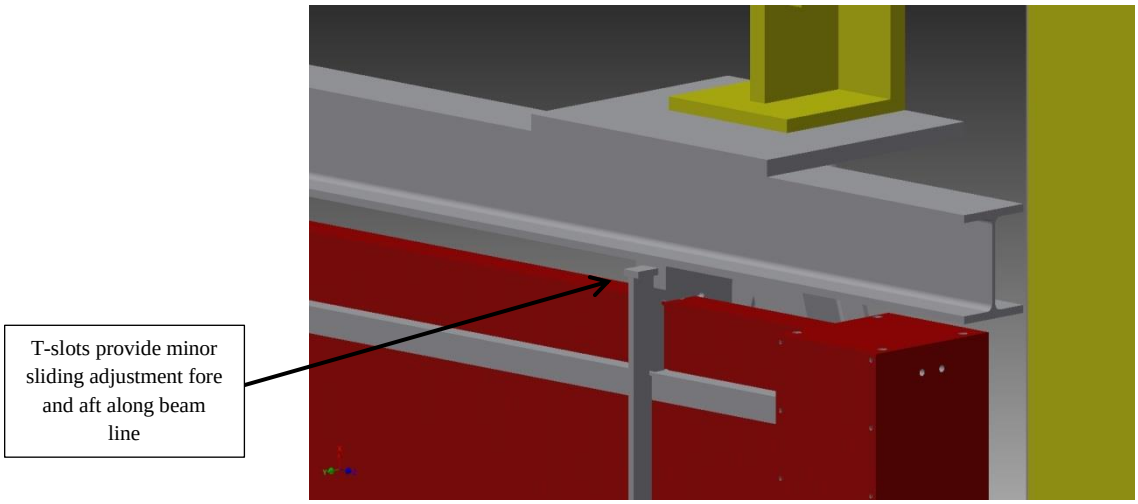

Figure 10 Detail view of bulkhead T-slots

The proposed horizontal frame will also allow relatively easy loading of the bar boxes into the support structure. Bar boxes will be slid into place, much in the same manner they were loaded into the original BaBar Detector. Figure 11 shows the method in which this was achieved.

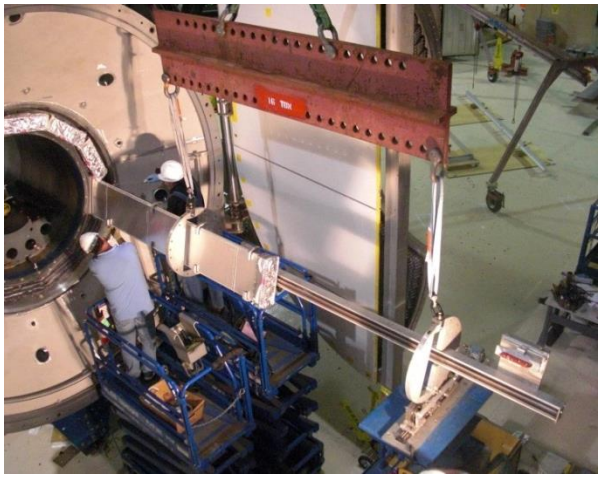

Figure 11 Showing bar box and special lifting fixture, in use during BaBar Detector Assembly

Figure 12 Specialized lifting and positioning fixture for bar boxes

The lifting fixture shown has the ability to rotate the bar boxes the necessary 90° for integration into the GlueX support structure and retain them while the being slid into place. The existing design is comprised of common materials and components, thus fabrication of a second fixture for use at JLab should be fairly straightforward.

SHIPPING CONTAINER DEVELOPMENT

When the DIRC BaBar detectors were originally constructed, the final assembly of the bar box components occurred on-site at SLAC. Between assembly in a clean room and installation into the experiment, the detectors were transported by means of a rigid lifting beam suspended from a forklift. The bar box was carefully lifted, moved at walking speed the distance between buildings, and put in place.

Figure 13 – Rigid lifting beam and bar box – SLAC

Since the bar boxes must be moved over 3,000 miles to Jefferson Lab, a reliable crating system must be designed from scratch. Several requirements must be met along the way. The bar boxes must remain around room temperature at all times, to prevent gross amounts of material expansion and contraction. Along with this the interiors of the boxes are to be under a continuous nitrogen boil-off purge. The nitrogen prevents ambient moisture from entering the boxes, along with dirt and contaminants.

Regarding the shock and vibrations induced from transport, acceleration forces of 3.0g or less are desired in all directions. The nylon buttons which support the fused silica bars internally were originally designed to slip and allow slight movement of the bars. Any minor shock to the bar boxes would thus be absorbed.

Air transport of the boxes logically appears to be the best method of conveyance, yet one detail complicates this. The aluminum honeycomb panels used in the outer bar box skins does not have equalizing orifices between the cells. That is, the honeycomb has no means of pressure equalization to compensate for lower atmospheric pressures at high elevation. If the bar boxes are to be transported by air it will be important to move them in a pressurized area of the cargo plane.

In order to thoroughly develop a suitable shipping crate it was determined that a full sized replica of the bars boxes, equal in size and weight, should be built. Fortunately the specific weights of Corning fused silica and 6061 aluminum bar stock are roughly the same, around .08 $lb./in^3$. A simplified design for a bar box was created by the team at IU, comprised almost entirely of aluminum. Attention was paid to ensure the weight distributions were similar between the actual and mock bar boxes along the long axis.

The mock bar box retains many of the same mechanical features that are present in the working bar boxes (as shown in the following figures). The replica retains the X-beam features, placed in the same locations. Aluminum plate and open cell honeycomb were used in the appropriate areas. While the mock box does not include the nylon buttons for retaining the bars, fasteners used to retain the aluminum skin are placed in comparable locations, and are sized similarly as well.

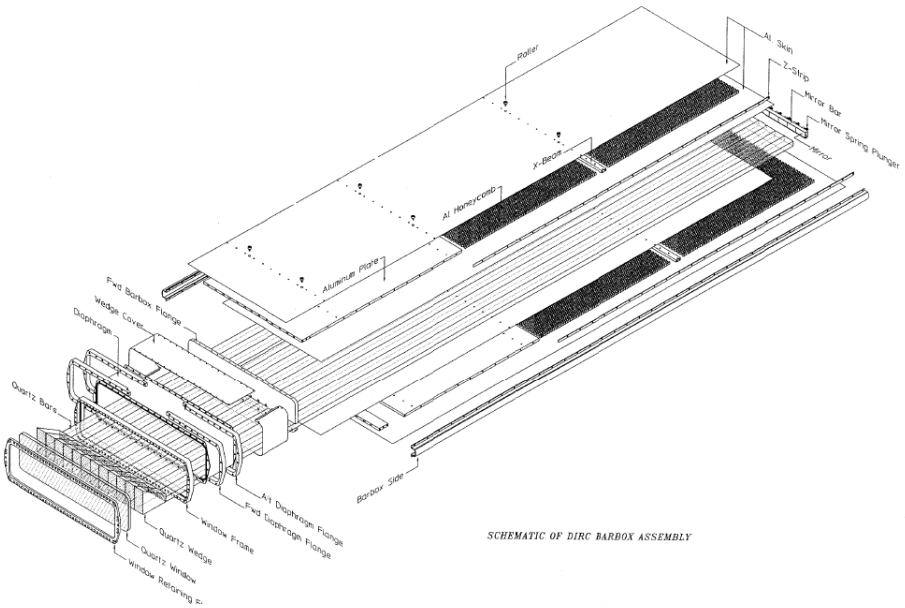

Figure 14 – Working bar box schematic

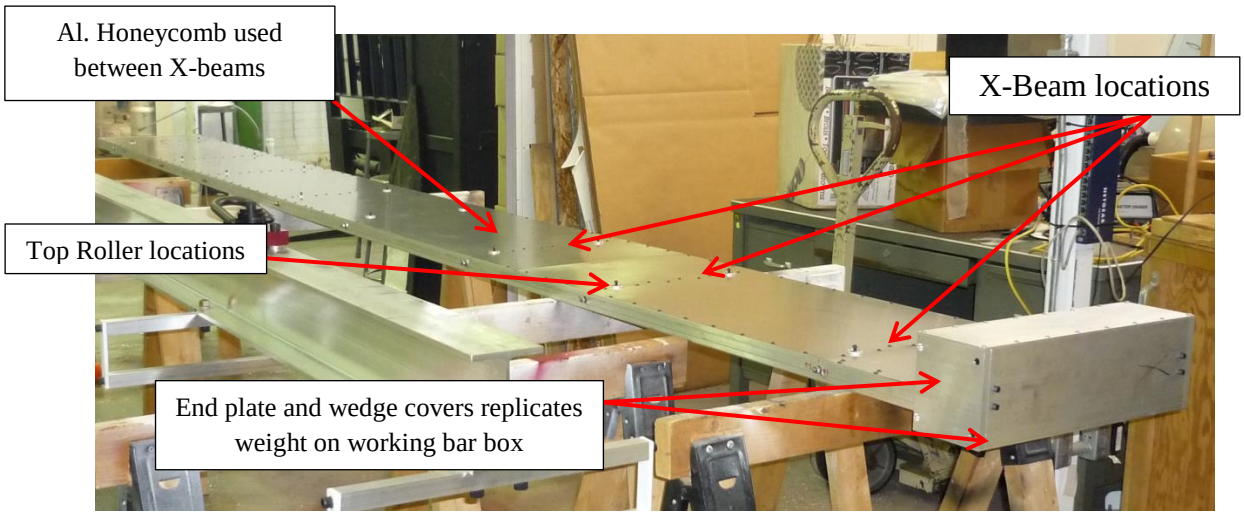

Figure 15- Mock bar box, showing design similarities

Figure 16 – Roller detail

Outside of large shock loads induced upon the bar boxes during transport, the other area of concern is the effect of naturally occurring vibration within the truck. It is critical that any vibration dampening materials be tuned to attenuate vibrations within certain frequencies that typically occur inside a semi-trailer. Several sources state semi-truck suspensions have a typical vibration frequency range of 2-7 Hz. Tire vibration usually occurs in the 15-20 Hz range, and structural vibrations occur in the 50-70 Hz range.

For a close approximation of resonant frequency for the mock bar box, the natural frequency equation for beams with uniform sections and uniform load can be used, that is;

Uniform beam uniform load natural freq. = $\omega_n = A\sqrt{\frac{EI}{\mu L^4}}$

Where: E = Young's Modulus = 10 EE 6 psi for Al.

I = area moment of inertia = 4.22 in^4

L = length of beam = 192 in

μ = mass per unit length of beam = 1.17 lb/in

A = constant for end conditions = fixed ends = 22.4 for Mode 1, 61.7 for Mode 2, and 121 for Mode 3

The results for these figures are as follows:

Mode 1 $\omega_n =$ 3.65 Hz

Mode 2 $\omega_n =$ 10.05 Hz

Mode 3 $\omega_n =$ 19.71 Hz

(Formula from "Natural Frequencies for Common Systems", University of Massachusetts Lowell)

From the given results, it is obvious that the tire and suspension vibrations present in typical semi-trailers will be of concern during bar box transport.

In further study of the natural resonance modes present within the mock bar box, some resonance testing was conducted using accelerometers to record acceleration values induced by hammer strikes. The data from the accelerometers was later reviewed using Fourier analysis. A number of X16-1D accelerometers were procured from Gulf Coast Data Concepts (http://www.gcdataconcepts.com/xlr8r-1.html). Figure 17 shows the set-up for the resonance test.

Figure 17 – Showing resonance test set-up for mock bar box

During the resonance test ten of the accelerometers were attached to the mock box, set to sample at 400 Hz. Due to the length of the mock box and the lifting equipment available, it was necessary to suspend the box from slings placed approximately four feet from each end. The box was slung in this manner to attempt to reduce any outside influences on the acceleration data. Hammer blows were first applied to the wedge end of the bar box, followed by manual lifting of the center of the box and allowing it to react for several seconds. Finally a series of hammer strikes were made on the mirror end of the bar box.

The data from the test was analyzed by means of ……..

Since the team at IU was not experienced in constructing large shipping containers, they looked for outside help in getting started. The requirements of moving the bar boxes made the search for advice a bit difficult. Ultimately assistance was found in the staff of Rock-It Cargo Co., a logistics firm that specializes in transporting delicate, irreplaceable goods around the globe, often with tight schedules and demanding requirements. Much of the work that Rock-It caters in deals with moving large and expensive works of art. Rock-It is not only a transport firm but deals with all aspects of a move including crate construction, packing, loading and unloading, etc. For crating consultation Rock-It referred IU to their primary crating contractor, Art Crating Los Angles or ACLA. ACLA sent a construction manager to IU for on-site consultation, to view the mock bar box and discuss the requirements. After several weeks of communication and construction, ACLA delivered a prototype crate assembly to IU.

Figure 18 – Museum quality bar box prototype crate, as delivered by ACLA

ACLA factored in the many requirements of the bar box move, and built a high quality crate that is capable of meeting many of the needs. The crate is essentially a "crate within a crate", providing ample rigidity to prevent any flexing along the length of the bar box. The entire assembly can be fully taken apart to make loading and unloading relatively easy.

Figures 19 and 20 - showing the ample room with the prototype crate system and ease of loading

The bar box rests on a bed of relatively dense multi-layer Volara foam. The foam is strategically placed within the crate to support the bar boxes at the X-beam locations. It also has cut-outs to allow the lifting fixture components to be removed once a lift is complete. The bar box is retained within the crate by means of foam covered cribbing blocks, which surround the box at various points and are attached with wood screws. When initially delivered the inner crate sat on five blocks of dense closed cell white foam, as shown in Figure 19 above. This same foam is also placed around the perimeter of the inner box, between it and the outer crate. The outer crate rests on round air doughnuts, "Skid Mates", that provide some shock absorption. The entire assembly, including the mock bar box, weighs approximatelyz 1560 lbs.

CRATE TESTING

For basic shock testing it was decided that simple drop tests would allow the IU team to observe the attenuating properties of crate system, with the end goal of performing an over the road test. All of the crate tests have involved dropping the one end of the crate from a height of 1.5 inches, off the end of a forklift fork. Accelerometers are mounted both on the lid of the crate and on the bar box itself. Thus the effectiveness of the entire crate system can be observed.

The first drop test performed in this manner quickly revealed that the crate as delivered was not satisfactory. The white closed cell foam did little to attenuate the shock from the drop, actually magnifying the initial impact. The drop from the second test is shown in Figures 21 and 22. It should be noted that all of the plots show acceleration for the vertical axis only, and are corrected for the gravitational constant; the values shown purely represent the impacts and the reactions themselves.

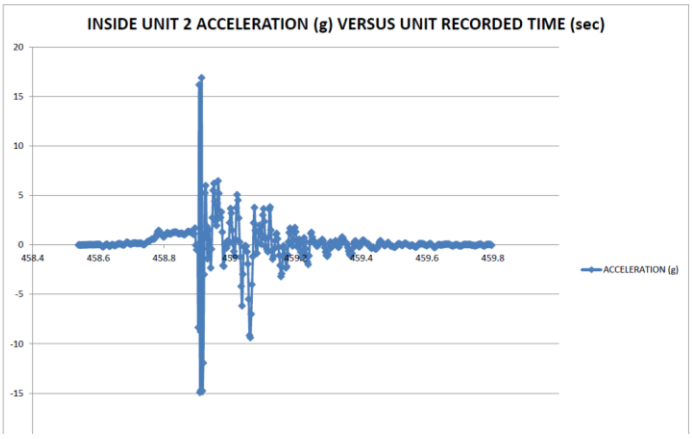

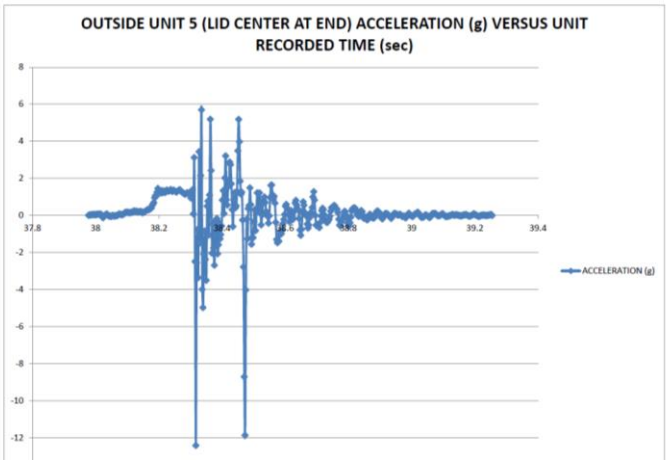

Figures 21 and 22 showing inner and outer crate accelerations respectively for the unmodified bar box crate

Several more tests were conducted in an attempt to improve the foam support, first by removing some of the foam from under the inner crate, then by adding foam under the lid. The material under the lid acted to compress the foam under the inner crate, essentially increasing the load the bottom material experienced. The hope was by increasing the load the material would

respond by increasing displacement on impact. Some attenuation began to appear, as shown in Figures 23 and 24, around 1.5 g's. However it was still far from practical.

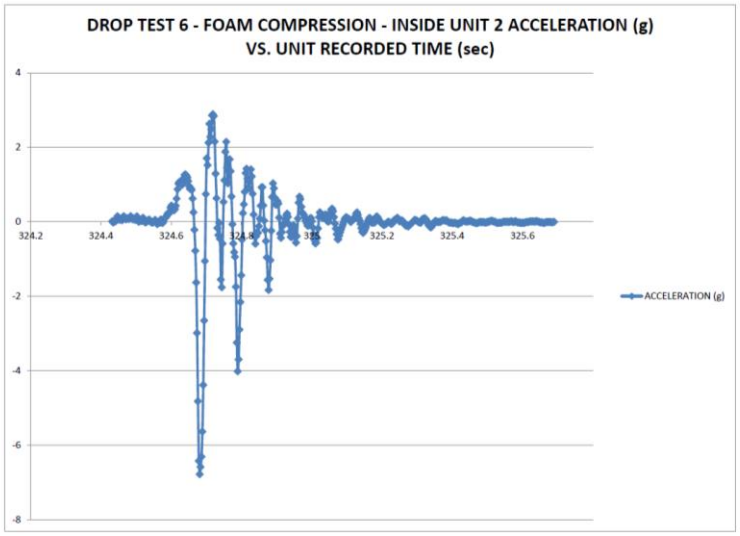

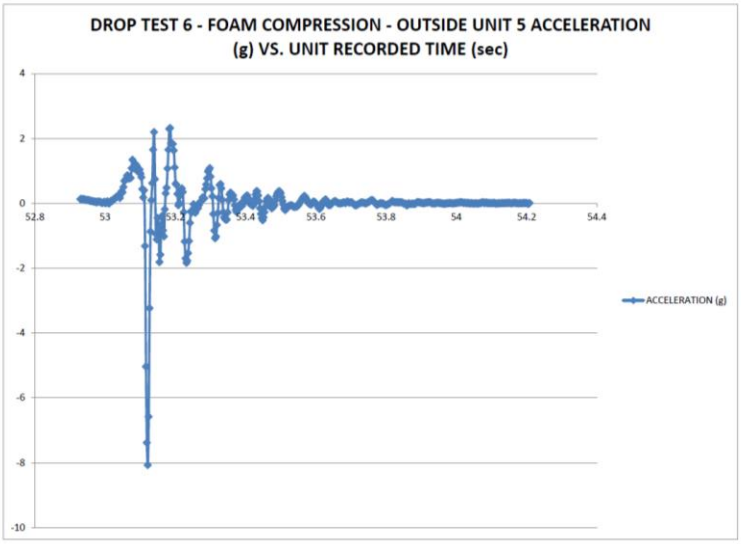

Figures 23 and 24 showing inner and outer crate accelerations respectively – an approximate 1.5 g attenuation

At this point it was decided to abandon the foam supports altogether and turn to a more adjustable and responsive option. Eight Goodyear brand mini sleeve style air springs were procured, designed to carry loads from 5 lbs. to 600 lbs. dependent upon inflation pressure. The air springs were mounted to the bottom of the inner crate by means of 2 in. square steel tube mounts, lag screwed to the bottom of the crate. Air springs were mounted at each end of the crate, as well as approximately 5 ft. from each end, alongside existing supports. The particular air springs chosen have a pressure range from 0 psi up to 100 psi. While they act to absorb shock they also have some minor vibration absorbing properties. For the given load they carry it was determined from the manufacturer's literature that for the best attenuation the inflation pressure would most likely be somewhere between 30 and 50 psi. For the initial drop test using

the air springs, pressure was set at 45 psi. A drastic improvement was recognized over the foam, as shown in Figures 24 and 25.

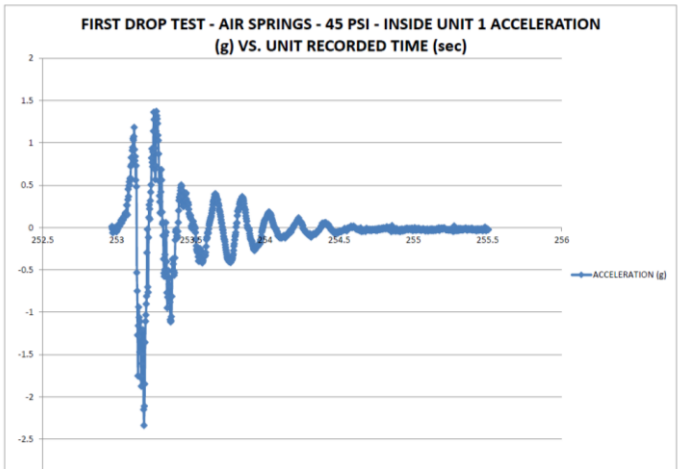

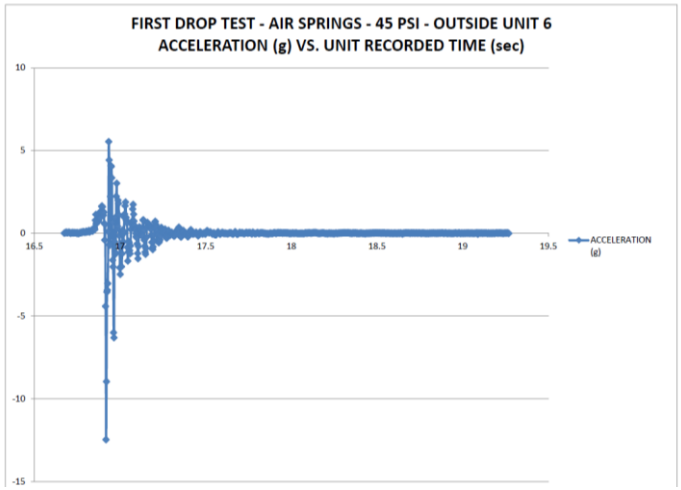

Figures 24 and 25 showing inside and outside accelerations respectively – note the 10 g reduction in acceleration

The air springs provided a great deal of shock absorption, around 10 g from inside to out during the simple drop tests. While the shock was lessened a great deal the amount of oscillation experienced by the inner crate after the impact remained a cause of concern. Figure 24 shows a very pure un-damped oscillation. In determining the amount of damping force required to critically damp the inner crate, it was necessary to first determine the calculated natural frequency of the crate assembly. To find the natural frequency, ω_n:

$$\text{System natural freq.} = \omega_n = \sqrt{\frac{K}{m}}$$

Where:

K = system spring rate at specific air pressure = empirically determined to be 1019 lb/in at 45 psi.

m = system mass = 789 lb. / 386 in/s^2

Solving for ω_n = 22.3 rad/sec

The critical damping force, C_c, was then determined:

$C_c = 2m\,\omega_n$ = 91.1 lb. – s. / in.

To critically damp the inner crate it would require a total damping force of approximately 90 lb. - second per inch, when the air spring pressure was set at 45 psi. Logically the choice was made to obtain four dampers and place one at each corner of the inner crate. Since it was desired to have some adjustability in the dampers, variable strength oil dampers were procured. The dampers chosen are capable of forces between 2 lbs. and 112 lbs., adjustable by means of threading/unthreading a valve connected to the piston rod. The dampers are of the extension acting type, that is, they dampen during extension and not on compression. This was done so as to ensure the air springs would continue to absorb shocks properly. Aluminum mount brackets were fabricated and lag screwed to the crates, after which the dampers were attached. Figure 26 shows the air spring and damper arrangement, common to all four corners.

Figure 26 - showing air spring and damper – outer crate side removed for view

Since it was relatively certain that 45 psi would be the maximum amount of inflation pressure used in the air springs, 90 lbs. of damping force would also be the maximum amount of damping force required. For the first drop test where the air springs and dampers would both be in use, the inflation pressure was set at 45 psi, and the damping force was set at a mere 7-8 lbs. per damper. Figures 27 and 28 show the results of the initial test:

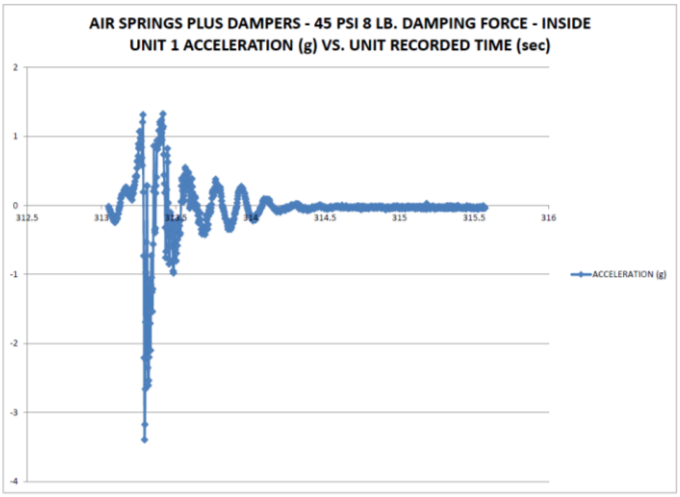

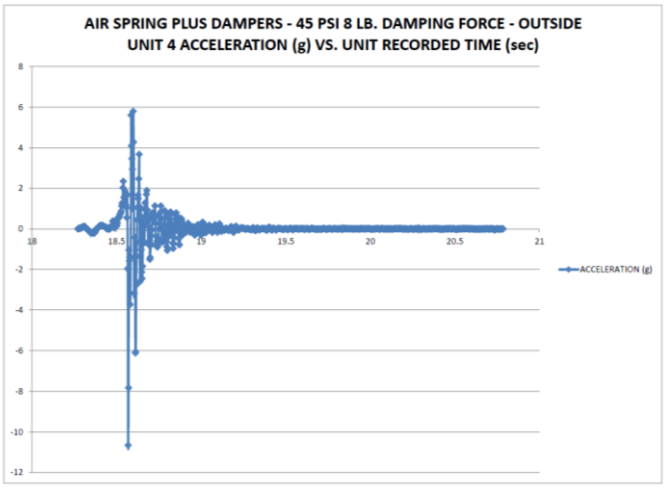

Figures 27 and 28 showing the inner and outer accelerations respectively for the first air spring and damper drop test

Comparing Figure 27 with Figure 24 in the un-damped air spring test, some attenuation of the oscillation is noted. However it is also of note that the impact acceleration values in the damped test increased substantially over the un-damped test. In the follow up test the inflation pressure in the air springs were reduced to ~32 psi.

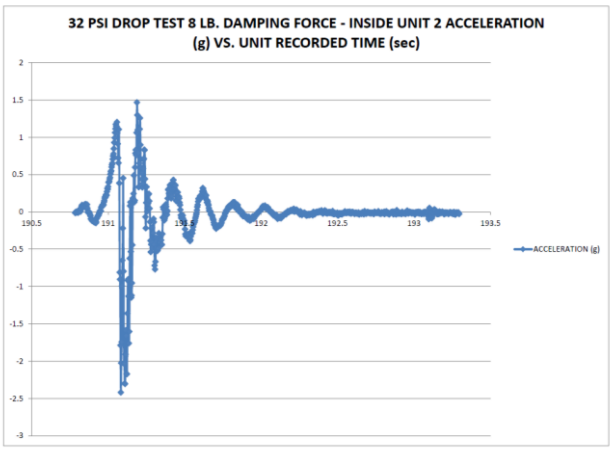

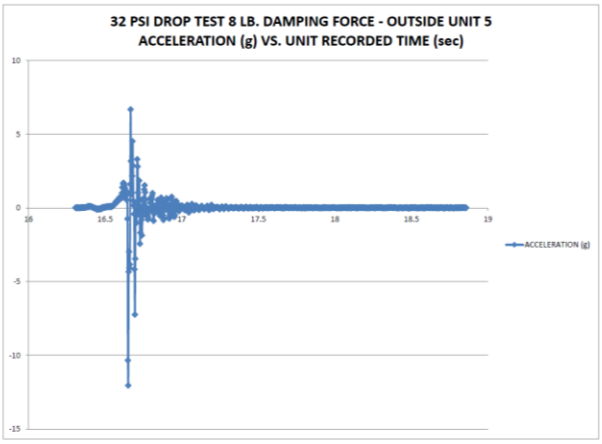

Figures 29 and 30 showing inner and outer acceleration values for the first reduced pressure drop test, respectively

Dropping the inflation pressure of the air springs from 45 psi to 32 psi effectively reduced the maximum acceleration at impact back to levels similar to those with no damping force. Yet the following oscillation was diminished to a degree. In an effort to observe a more extreme set up, the inflation pressure in the air springs was dropped to 24 psi, much below the vibration attenuation range recommended by the manufacturer. Damping force was also increased to ~20 lbs. per damper, very close to the calculated critical damping force required at the higher inflation pressure.

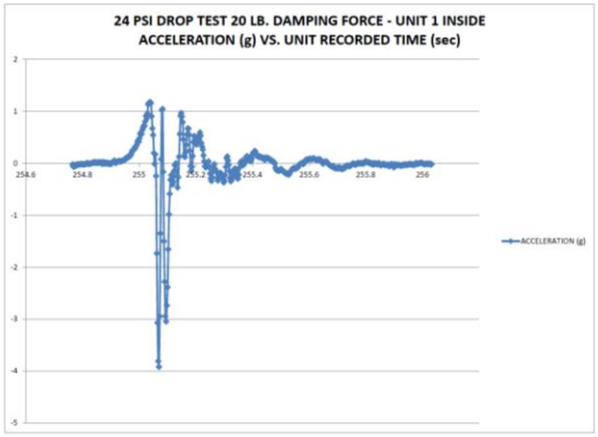

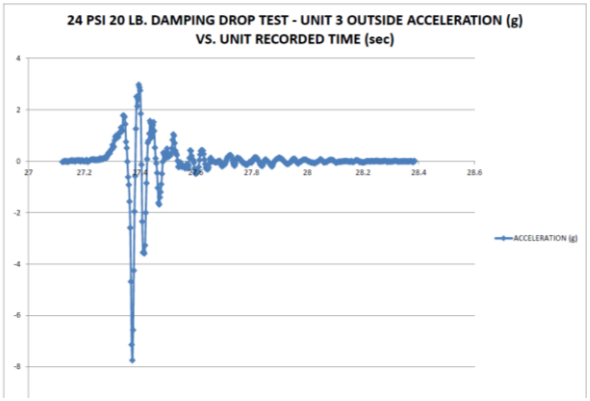

Figures 31 and 32 for the approximate critically damped inner crate and outer crate, respectively

Figure 32 shows the acceleration value at impact for the inner crate, with a nearing critically damped oscillation following. While this resulted in a near successful test from a damping standpoint, the effect on the acceleration at impact can clearly be seen. In typical spring-damping systems it is generally desirable to slightly under-damp the system, in an effort to minimize any initial impact. Thus the next test run was to slightly increase the inflation pressure of the air springs, to 25-26 psi and reduce the damping force to ~12 lb.

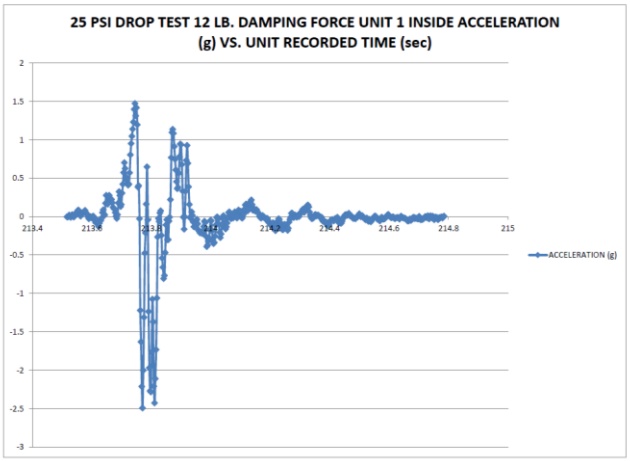

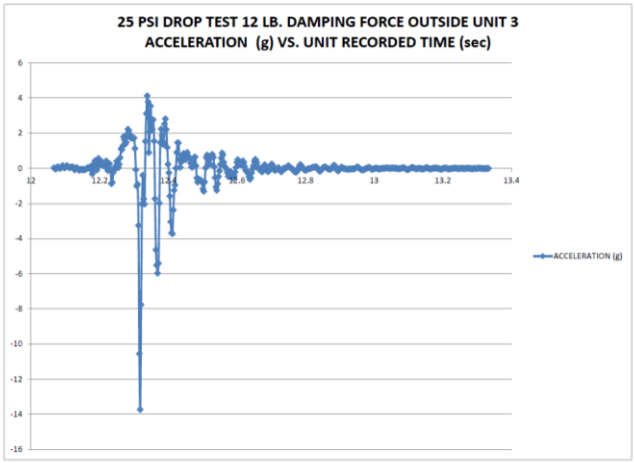

Figures 33 and 34 showing the reduced damping drop test, inner and outer acceleration values respectively

Figure 33 shows a closer to ideal set up for the inner crate. While the system is underdamped, the oscillation dies fairly quickly. Yet the initial impact acceleration is kept below 2.5 g's inside, as the outer crate experiences a near 14 g acceleration.

INITIAL ROAD TEST

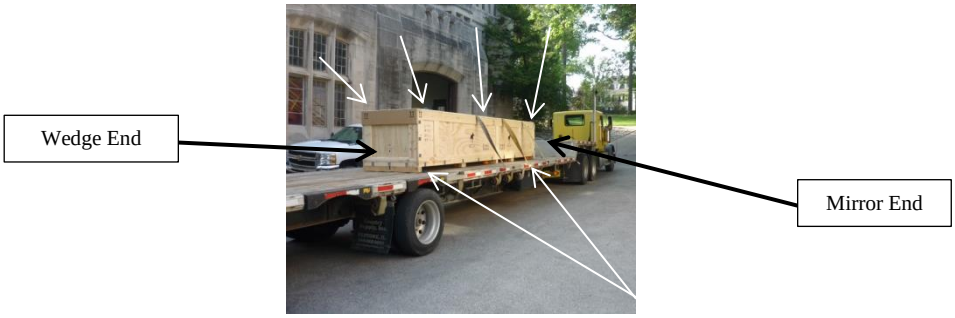

Figure 35 - Initial road test equipment and set-up; arrows denote accelerometer locations, both on the truck bed and on the crate. Orientation of the bar box is also noted. Accelerometers were also placed inside on the bar box, in approximately the same locations as those on the outer crate

An initial road test was conducted on May 27, 2015. The trailer used was an air ride flatbed type. This type of trailer was chosen over a van type trailer to simplify loading and unloading. The crate was placed on the bed just ahead of the forward most rear axle, in an attempt to set it at the smoothest riding point on the trailer. The test run ran on local highways to Interstate 69 then preceded between Bloomfield and Washington, Indiana. After exiting at Washington, the truck ran on US Highway 50 east to Bedford, Indiana. Here the truck turned north and returned to Bloomington via Indiana 37, a four lane highway. The test run lasted approximately four hours. The entire test went as planned, with one issue; the end joint on the right side damper on the mirror end of the inner crate unthreaded and fell apart at some point during the trip. This was later remedied by a few drops of Loctite. Thus for part of the trip the inner crate was only 75% damped.

During the road test the settings for the air springs and dampers were set at 32 psi and 8 lbs. respectively. These settings were used at this time, as it appeared they might be the most

effective. The results from the road test however, showed otherwise. Generally speaking for most of the higher (3g+) accelerations induced on the trailer, the acceleration inside the box would be reduced by 50%. The highest acceleration seen across the entire test is shown in Figures 36 and 37, showing the trailer and box accelerations respectively.

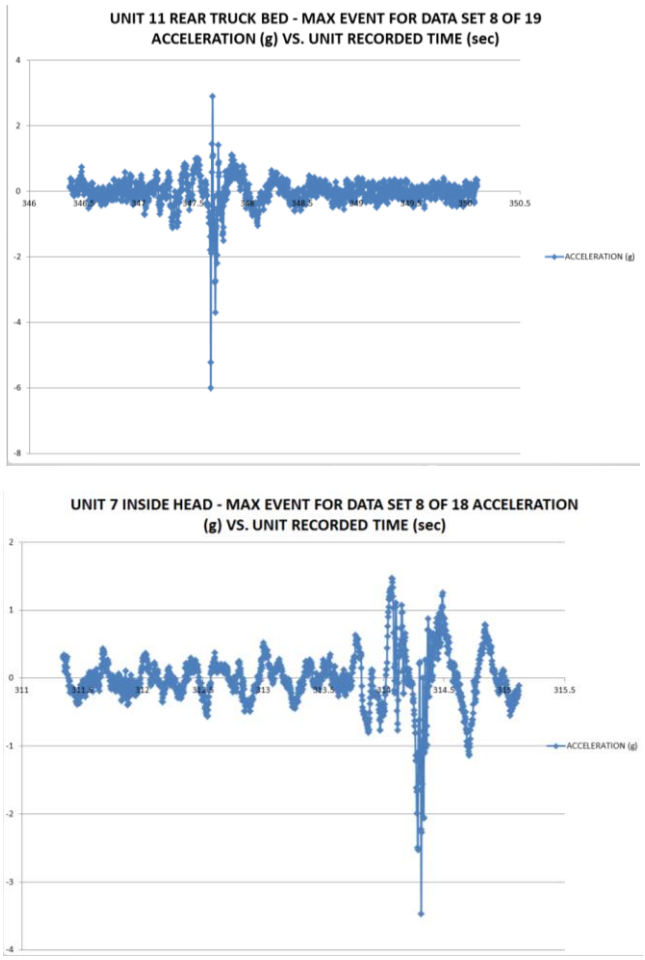

Figures 36 and 37 showing the -6g trailer acceleration, and the -3.4g acceleration within the box; this was the maximum acceleration event for the entire road test.

From the experience gained in the first road test, more static drop tests were conducted to further improve the crate's ability to absorb shock. The spring and damper settings of 25-26 psi and 12 lb.-in./sec. respective, were finalized. In an effort to further provide shock reduction, the decision was made to mount a set of air springs to the outer crate. A set of six air springs were procured, whose weight capacity range was appropriate for the nearly 1600 lb. container.

Figure 38 showing one of three outer crate suspension members

It was hoped that the second pair of air springs under the outer crate would provide an additional layer of shock absorption for the container; however the results were mixed in the static drop tests and the addition of the outer springs proved marginally successful. Half a dozen drop tests were performed to find the optimal air pressure settings. The results of those tests are shown in Figures 39 and 40.

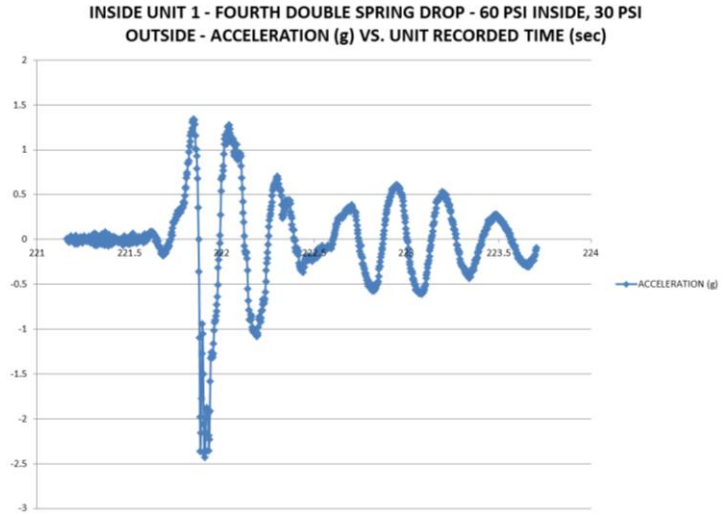

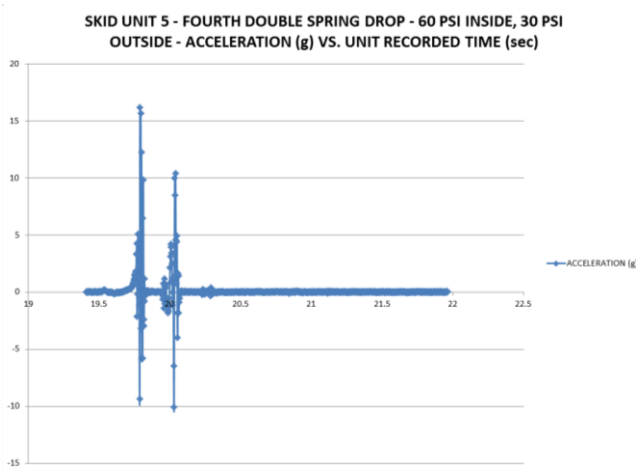

Figures 39 and 40 showing the inner and outer crate accelerations respectively; the plots shown represent the most optimal settings found with the double air spring set-up.

When comparing Figures 39 and 40 with Figures 33 and 34 it can be noted that the inner acceleration values are very similar, the peaks being slightly less with the double spring set-up at best. The immediate problem noted was the difficulty in controlling the amount of oscillation following a shock event, at the air pressure settings required. Given the complexity of maintaining the outer springs, along with considerations about crate restraint during transportation, the decision was made to take a step back and eliminate the outer spring set. Focus was then put on finding ways to improve the ride qualities of the semi-trailer.

SECOND ROAD TEST

Figure 41 showing trucking equipment and set-up of second road test

Another round of road testing was conducted with the crate on Wednesday August 23, 2015. The test was conducted to measure the effectiveness of the optimal air spring and damper settings, found after the conclusion of the previous road test. Along with testing the new component settings, focus was put on experimenting with means of improving the ride quality of the trailer. For both road tests flatbed semi-trailers with air ride suspensions were used, both having a load capacity of 50,000 lbs. During the first test the crate alone was the only item on the trailer bed, thus in comparison to the capacity the load was very minute, only accounting for about 3% of the trailer's maximum capacity. To make an effort to improve the ride of the trailer

ballast weight was applied to the trailer bed. Three concrete blocks, each weighing approximately 3600 lbs., were loaned from another IU department. The blocks along with the crate brought the total load up to around 12,400 lbs., around 25% of the capacity of the trailer. It was felt by several members of the research team that adding ballast to the trailer would greatly improve the ride quality, based on prior experience with trucking suspension systems.

The road test began at 8 A.M. and lasted for around four hours, covering the same route as the previous test; local roads, a newly constructed interstate highway, followed by several two and four lane state highways. Figures 42-45 below show the extreme events for both the interior of the crate and for the truck bed respectively. In both instances the acceleration values for the interior of the crate and truck bed are shown.

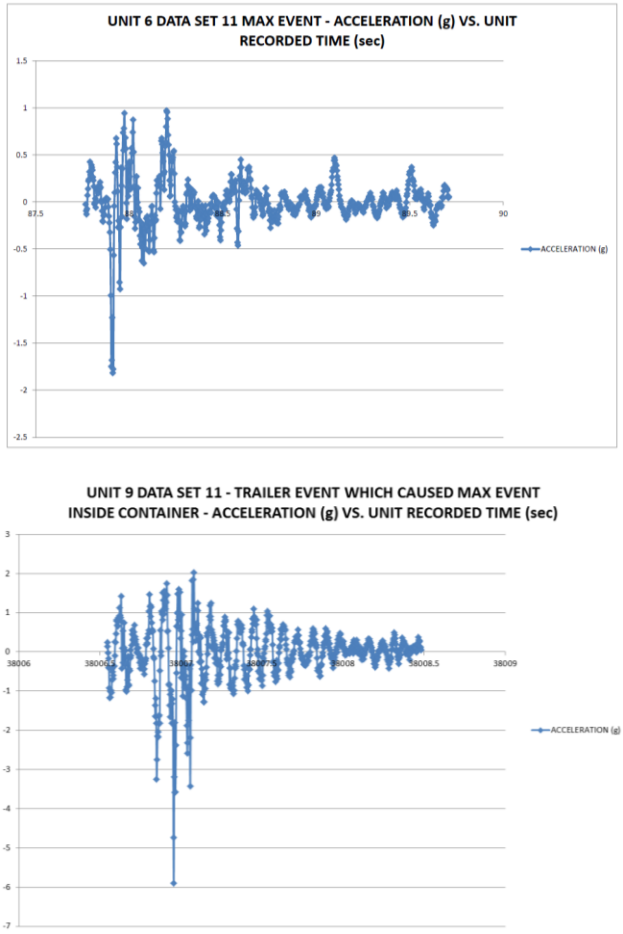

Figures 42 and 43 showing the event which produced the maximum Z axis acceleration within the shipping container, plots display inside the container (Unit 6) and the trailer bed (Unit 9) respectively

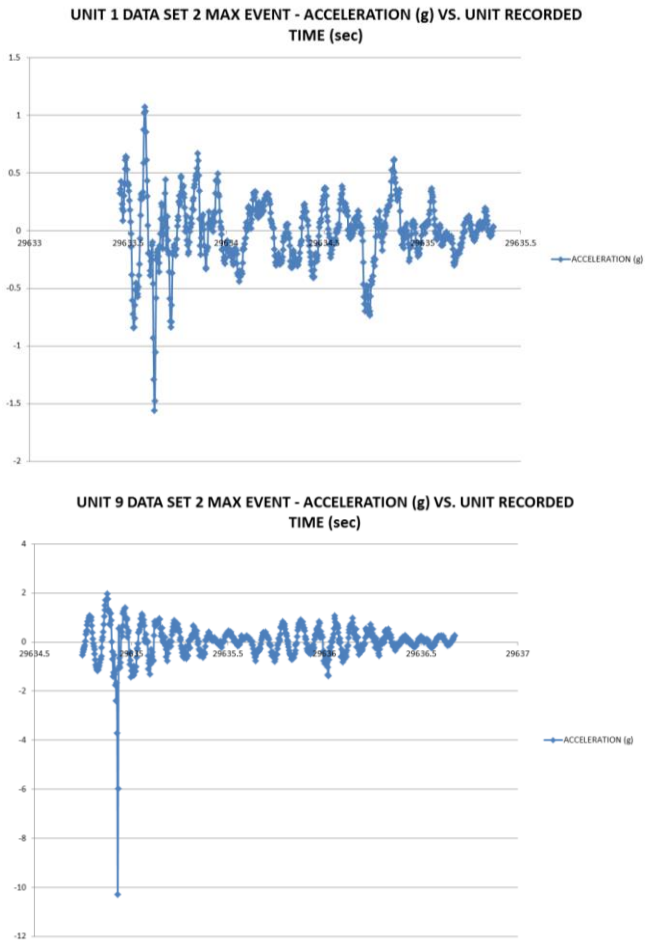

Figures 44 and 45, showing the event which produced the maximum acceleration on the trailer bed; plots display the values inside the container (Unit 1) and on the trailer bed (Unit 9) respectively

From the previous plots it can be seen that the maximum acceleration value witnessed inside the crate during the four hour test was around -1.8 g. The maximum acceleration seen on the truck bed was in excess of -10g. The refined spring and damper settings, along with the addition of mass to the trailer-crate system appeared to have made the difference. One interesting note regarding the maximum acceleration of the truck bed is that the values recorded during this test were far greater than those of the first test. The maximum acceleration during the first test, shown in Figure 36, is around -6g. Several times during the second test the truck bed experienced greater acceleration, as shown in Figure 40, well in excess of -6g. However the oscillation following the impact, the "bouncing" of the trailer, was reduced during the second test by the addition of the concrete ballast. Ensuring the trailer is loaded with sufficient weight, to force the suspension system to function within its operating range, seems to be a critical step in seeking a smooth riding transport system.

The primary focus of development work with the crate has been on reducing the vertical (Z axis) accelerations and impacts. This is due to the fact that the bar boxes and the glass bars within are arguably most delicate in this orientation, the position they must be transported in. During the testing however the other two axes have been monitored, fore and aft (X axis) and lateral (Y axis). During the second road test the accelerations in the X axis were consistently

low, usually around ±.25g-.4 g. The peak X acceleration during the entire test was .56g. A long truck-trailer wheel base helps maintain these low values. Accelerations in the Y axis, however, are somewhat greater. Typical figures for the Y axis accelerations are ±.5g – 1.5g. Over the course of the four hour road test, acceleration values consistently ran within this range, with one or two notable exceptions. The maximum outlier for the Y axis acceleration was -2.77 g, as detailed below in Figures 46 and 47.

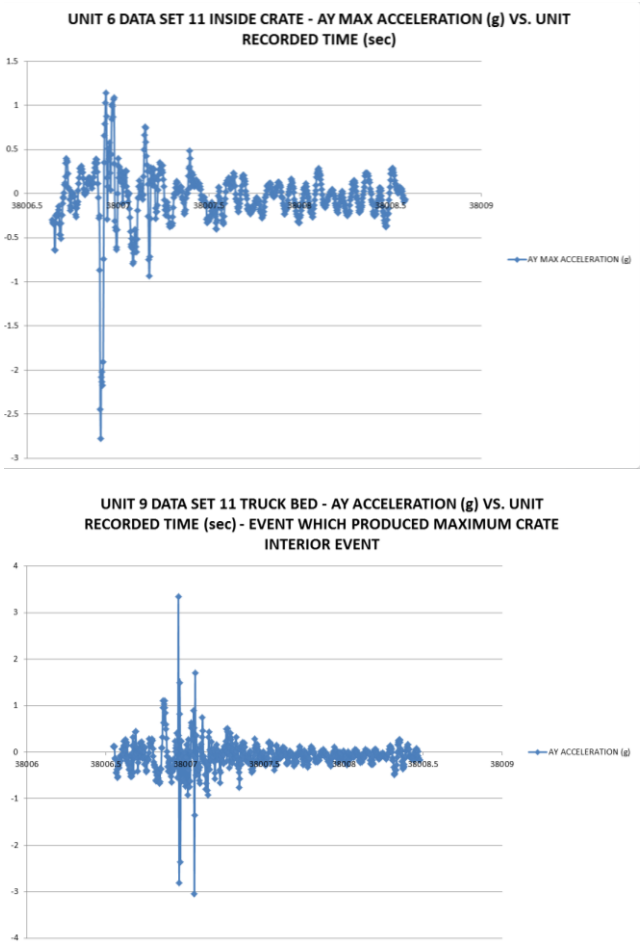

Figures 46 and 47, showing the Y axis maximum acceleration values for the interior of the crate and the truck bed, respectively

The air springs used on the inner crate offer great shock reduction in their primary axis of operation, the Z axis. They do offer fore and aft and lateral reduction as well, this being an inherent quality. The above event shown in Figures 46 and 47 was the maximum outlier of the entire test, most likely caused by the tires on one side of the trailer hitting a large hole. This event was also responsible for the maximum Z axis event, detailed in Figures 42 and 43. While it is felt that this was an unusual event, steps should be taken when building future crates to prevent such accelerations from making their way to the bar box. The addition of an air spring at each of the four corners on the inner crate, oriented laterally against the side of the outer crate and inflated to a low pressure, would most likely eliminate large acceleration as witnessed above.

In conclusion regarding the air springs used under the inner crate; the particular air springs used are very effective in reducing large accelerations and impacts. From the static drop tests, as shown in Figures 33 and 34, these air springs are capable of reducing -14 g outer crate accelerations down to -2.3 g inside. Their performance suffers however when subjected to high impact events in the midst of high vibration periods (think bridge expansion joints in the midst of very rough roads). To help with this issue it is important that the trailer the crate is transported on be loaded with an appropriate amount of weight in comparison to its maximum rating. This forces the trailer suspension to operate within its effective design range and reduces the amount of bouncing that is inherent in light load situations. In regards to their robustness the air springs are fairly maintenance free, however they are known to develop minor air leaks around the supply fittings. Some of the springs stay inflated at the set pressure for several weeks, others last only a few days. It is recommended that in the future all air springs be plumbed together, and be supplied with a reserve bottle outfitted with a pressure regulator. The reserve bottle could be charged with air at 125 psi, with the regulator set at 25-27 psi. In this manner a sufficient supply of air could be delivered to the air springs for a number of days, to overcome any minor leak. As a final refinement in future crates four air springs, oriented laterally and one positioned at each corner, should be put in place to reduce any outstanding Y axis accelerations.